Nonvolatile Nanopipelining Logic Using Multiferroic Single-Domain Nanomagnets

Yalcin Yilmaz and Pinaki Mazumder, *Fellow, IEEE*

***Abstract*— Multiferroic single-domain nanomagnetics is a promising emerging nanotechnology poised to usher in ultralow energy nanomagnetic nonvolatile logic circuits in numerous medical applications, such as implants and prosthesis, where battery longevity is paramount. This paper evaluates the fundamental mode of signal propagation over ferromagnetically and antiferromagnetically coupled wires and interaction between the magnetic nanoparticles to perform nonvolatile logic functions, such the majority gate that sets its output to 1 when the majority of the inputs is 1. By taking advantage of magnetic nonvolatility, the paper demonstrates nanopipelining signal processing, data propagation performance, and functionality of basic building blocks. Our results indicate that effective nanopipeling can be achieved with clock periods approaching 9 ns and energy dissipation of 20 aJ per nanomagnet switch with the device sizes considered.**

***Index Terms*— Nanomagnetic logic, nanopipelining, straintronics.**

I. Introduction

NANOMAGNETS offer inherent nonvolatility, radiation hardness, and high-integration densities, which make them attractive for various applications [1]. Nanomagnetic logic using nanomagnets as computing elements has emerged as a new ultralow energy paradigm for digital computation as an alternative to CMOS [2]. Several researches have been performed in this field to develop nanomagnetics-based technologies [1]–[5].

The elliptical multiferroic single-domain nanomagnet is the interest of this paper [3]. Elliptical nanomagnets are bistable devices that allow the stable magnetization directions to encode bits "0" and "1." Nanomagnetic logic relies on the alignment of nanomagnets when there is magnetization orientation change in one or more of input nanomagnets. In order to allow unidirectional propagation of data through magnetically coupled elliptical nanomagnets, a clocking scheme is required. Multiple approaches are proposed to generate clocking schemes, such as the use of local or global magnetic fields to ensure data propagation along the bias direction [4], [5]. Another approach recently proposed in [3] is to use multiferroicnanomagnets to achieve local clocking. These devices consist of a magnetostrictive layer, whose magnetization can be rotated via applied stress, and a piezoelectric layer, which can transfer the required stress to the magnetostrictive layer when a voltage is applied across it. Multiferroic single-domain nanomagnets have been recently shown to be energy efficient for nanomagnetic logic applications that potentially require lower energy dissipations than spin transfer torque [6].

Operational devices consisting of magnetostrictive and piezoelectric layers have been manufactured. Brintlinger *et al.* report stress-generated switching in electromechanically coupled thin film $Fe_{0.7}Ga_{0.3}/BaTiO_3$ bilayer structures in [7], and Chung *et al.* report control over metastable magnetic single domain using inverse magnetostrictive effect in Ni-nanobar/lead zirconatetitanate (PZT) film devices in [8].

In this paper, we investigate the possible pipelining approaches using these devices, as well as performance based on data propagation orientations and the functionality of the basic blocks. This technology has been evaluated for antiferromagnetically coupled binary wires, but a working majority gate also needs to be analyzed. We found out that in this technology, it is not possible to make a majority gate work if main components are ferromagnetically coupled. Also, switching performances for binary wires and the majority gate are not the same.

II. Pipelining of Nanomagnetic Logic

A. Building Blocks

Basic building blocks of nanomagnetic logic are obtained with various arrangements of nanomagnets, which are magnetically coupled to their nearest neighbors [2]. A linear (vertical/ferromagnetic or horizontal/antiferromagnetic) arrangement of these wires comprises a "binary wire" if the number of nanomagnets is odd, and they form an inverter or an "inverting binary wire" if the number of nanomagnets is even (only in horizontal arrangement). If vertical and horizontal arrangements are combined, a majority gate is obtained. Fig. 1 shows the realizations of these gates. These building blocks constitute the lowest level components. The components are symmetric in the sense that the data flow can happen in all directions, and not necessarily from input ports to the output. It is shown in many works [4], [5] that some sort of clocking scheme is essential to achieve unidirectional (input to output) dataflow.

When a nanomagnet is disturbed out of the equilibrium state, it is equally likely to align itself with either one of its neighbors when neighbors have opposite magnetization directions; caused by the fact that the dipole-dipole interaction

Manuscript received April 27, 2011; revised June 5, 2012; accepted June 15, 2012. Date of publication August 8, 2012; date of current version June 21, 2013. This work was supported in part by the National Science Foundation under Grant ECCS 1124714 and the SRC Award.

The authors are with the Department of Electrical Engineering and Computer Science, University of Michigan, Ann Arbor, MI 48109 USA (e-mail: yalciny@umich.edu; mazum@eecs.umich.edu).

Color versions of one or more of the figures in this paper are available online at http://ieeexplore.ieee.org.

Digital Object Identifier 10.1109/TVLSI.2012.2205594

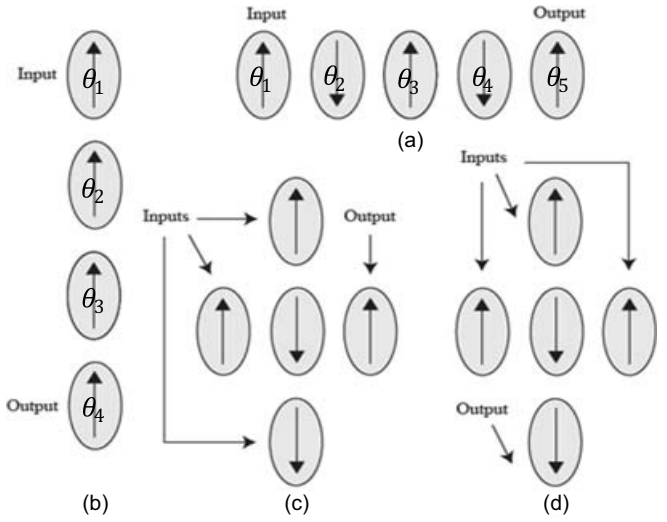

Fig. 1. Basic building blocks. (a) Antiferromagnetically coupled binary wire. (b) Ferromagnetically coupled binary wire. (c) Majority gate—output antiferromagnetically coupled. (d) Majority gate—output ferromagnetically coupled.

torque acting on the nanomagnet due to its neighbors is equal. In order to break the equilibrium and bias the nanomagnet toward the input neighbor, the torque due to the output neighbor should be reduced. This can be achieved by also disturbing the output neighbor out of the equilibrium and forcing its magnetization toward the hard axis, reducing the dipole-dipole interaction.

B. Ferromagnetic and Antiferromagnetic Alignments

Elliptical nanomagnets can be aligned along their hard or easy axes. Fig. 1 shows different alignments for a majority gate and different modes of nanomagnetic binary wires. In the binary wire cases, if wires are vertically aligned and vertically magnetized, ferromagnetic coupling is achieved; otherwise, if wires are horizontally aligned and vertically magnetized, antiferromagnetic coupling is achieved [9]. It is possible to configure the majority gate in two different ways, depending on the choice of the input and output nanomagnets. The output nanomagnet can be chosen to be ferromagnetically or antiferromagnetically coupled to the center nanomagnet.

Depending on the alignments, different switching performances can be obtained by utilizing the varying dipole-dipole interactions in different cases.

C. Device Properties

The devices of consideration [3], multiferroic single-domain nanomagnets, are composed of two layers with elliptical cross sections. The first layer is the magnetostrictive layer, which is the main nanomagnet body magnetically coupled to neighboring nanomagnets. The second layer is the PZT layer deposited on top of the magnetostrictive layer and applies stress to the bottom layer when a potential difference is applied across it. We use the materials and device characteristics as cited in Table I to generate our results.

D. Switching Dynamics

The magnetization switching dynamics of a nanomagnet is characterized by the Landau-Lifshitz-Gilbert (LLG) equation.

TABLE I
MULTIFERROIC NANOMAGNET MATERIAL AND DEVICE CHARACTERISTICS

Material and Geometry Parameters	
Magnetostrictive Material	Terfenol-D
Young's modulus (Y)	8×10^{10} Pa
λ_S	60×10^{-5}
M_S	8×10^{5} A/m
α	0.1
a	101.75 nm
b	98.75 nm
t	10 nm
PZT thickness	40 nm

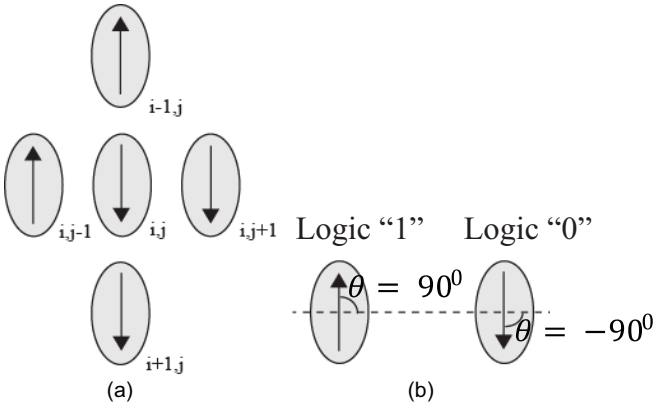

Fig. 2. (a) Majority gate. (b) State encoding.

The LLG equation can be numerically solved to evaluate the magnetization direction of a nanomagnet under the influence of dipole-dipole interaction with neighboring nanomagnets, shape anisotropy, external stress, and applied field (Zeeman) terms. The numerical method to evaluate the magnetization angle of a multiferroic single-domain nanomagnet is shown in [3]. We will expand the mechanism shown in [3] for the majority gate.

Switching characteristics of the central nanomagnet in Fig. 2 are dictated by dipole-dipole interactions due to its surrounding four nanomagnets, shape anisotropy, and applied stress. Atulasimha and Bandyopadhyay [3] provide details on assumptions and simplifications.

The dipole energies due to the vertical and horizontal couplings are

$$\mathrm{E}_{\mathrm{dipole\_horizontal}} = \frac{\mu_0 M_s^2 \Omega^2}{4\pi R^3}\left(\sin\theta_{i,j}\sin\theta_{i,j+1} - 2\cos\theta_{i,j}\cos\theta_{i,j+1}\right) \quad (1)$$

$$E_{\mathrm{dipole\_vertical}} = \frac{\mu_0 M_s^2 \Omega^2}{4\pi R^3}\left(\sin\left(\theta_{i,j}-\frac{\pi}{2}\right)\sin\left(\theta_{i+1,j}-\frac{\pi}{2}\right) - 2\cos\left(\theta_{i,j}-\frac{\pi}{2}\right)\cos\left(\theta_{\mathrm{i}+1,j}-\frac{\pi}{2}\right)\right) \quad (2)$$

where R is the center-to-center distance between nanomagnets, μ_0 is the permeability of vacuum, Ω is the volume of the nanomagnet and M_s is the saturation magnetization.

Therefore, the total dipole interaction energy is

$$\begin{aligned}
&E_{\text{dipole_total}} \\
&= E_{\text{dipole_horizontal}} + E_{\text{dipole_vertical}} \\
&= \frac{\mu_0 M_s^2 \Omega^2}{4\pi R^3}\Bigg(\sin\theta_{i,j}\sin\theta_{i,j-1} - 2\cos\theta_{i,j}\cos\theta_{i,j-1} \\
&\quad + \sin\theta_{i,j}\sin\theta_{i,j+1} - 2\cos\theta_{i,j}\cos\theta_{i,j+1} \\
&\quad + \sin\left(\theta_{i,j} - \frac{\pi}{2}\right)\sin\left(\theta_{i-1,j} - \frac{\pi}{2}\right) \\
&\quad - 2\cos\left(\theta_{i,j} - \frac{\pi}{2}\right)\cos\left(\theta_{i-1,j} - \frac{\pi}{2}\right) \\
&\quad + \sin\left(\theta_{i,j} - \frac{\pi}{2}\right)\sin\left(\theta_{i+1,j} - \frac{\pi}{2}\right) \\
&\quad - 2\cos\left(\theta_{i,j} - \frac{\pi}{2}\right)\cos\left(\theta_{i+1,j} - \frac{\pi}{2}\right)\Bigg). \quad (3)
\end{aligned}$$

Shape anisotropy energy of an elliptical nanomagnet is

$$E_{\text{shape}} = \left(\frac{\mu_0 M_s^2 \Omega}{2}\right)\left[N_{d_{xx}}\cos^2\theta_{i,j} + N_{d_{yy}}\sin^2\theta_{i,j}\right] \quad (4)$$

and the demagnetization factors are

$$N_{d_{xx}} = \frac{\pi}{4}\left(\frac{t}{a}\right)\left(1 + \frac{5}{4}\left(\frac{a-b}{a}\right) + \frac{21}{16}\left(\frac{a-b}{a}\right)^2\right) \quad (5)$$

$$N_{d_{yy}} = \frac{\pi}{4}\left(\frac{t}{a}\right)\left(1 - \frac{1}{4}\left(\frac{a-b}{a}\right) - \frac{3}{16}\left(\frac{a-b}{a}\right)^2\right) \quad (6)$$

where a and b are the major axes of the elliptical nanomagnet and t is its thickness.

Stress anisotropy energy due to external stress is

$$E_{\text{stress}} = -\frac{3}{2}(\lambda_s \sigma \Omega)\sin^2\theta_{i,j} \quad (7)$$

where $(3/2)\lambda_s$ is the saturation magnetostriction and σ is the applied stress.

The total energy of the nanomagnet is then given b

$$\begin{aligned}
&E_{\text{total}} \\
&= E_{\text{dipole_total}} + E_{\text{shape}} + E_{\text{stress}} \\
&= \frac{\mu_0 M_s^2 \Omega^2}{4\pi R^3}\Bigg(\sin\theta_{i,j}\sin\theta_{i,j-1} - 2\cos\theta_{i,j}\cos\theta_{i,j-1} \\
&\quad + \sin\theta_{i,j}\sin\theta_{i,j+1} - 2\cos\theta_{i,j}\cos\theta_{i,j+1} \\
&\quad + \sin\left(\theta_{i,j} - \frac{\pi}{2}\right)\sin\left(\theta_{i-1,j} - \frac{\pi}{2}\right) \\
&\quad - 2\cos\left(\theta_{i,j} - \frac{\pi}{2}\right)\cos\left(\theta_{i-1,j} - \frac{\pi}{2}\right) \\
&\quad + \sin\left(\theta_{i,j} - \frac{\pi}{2}\right)\sin\left(\theta_{i+1,j} - \frac{\pi}{2}\right) \\
&\quad - 2\cos\left(\theta_{i,j} - \frac{\pi}{2}\right)\cos\left(\theta_{i+1,j} - \frac{\pi}{2}\right)\Bigg) \\
&\quad + \left(\frac{\mu_0 M_s^2 \Omega}{2}\right) \times \left[N_{d_{xx}}\cos^2\theta_{i,j} + N_{d_{yy}}\sin^2\theta_{i,j}\right] \\
&\quad - \frac{3}{2}(\lambda_s \sigma \Omega)\sin^2\theta_{i,j}. \quad (8)
\end{aligned}$$

In order to determine the magnetization orientation of a nanomagnet under external influences, the LLG equation needs to be evaluated

$$\frac{d\vec{M}}{dt} = -\gamma\,\vec{M} \times \vec{H}_{\text{eff}} = \frac{\alpha\gamma}{M_s}\left[\vec{M} \times \left(\vec{M} \times \vec{H}_{\text{eff}}\right)\right] \quad (9)$$

where $\vec{M}$ is the magnetization of the nanomagnet, γ is the gyromagnetic ratio, α is the damping factor and $\vec{H}_{\text{eff}}$ is the effective magnetic field on the nanomagnet and $\vec{H}_{\text{ext}}$ is described by the equation

$$\vec{H}_{\text{eff}} = \frac{1}{\mu_0 \Omega}\frac{dE}{d\vec{M}} + \vec{H}_{\text{ext}} \quad (10)$$

where E is the total energy of the nanomagnet due to the shape anisotropy, stress anisotropy and dipole-dipole interactions and is the external magnetic field.

Since the nanomagnets have diameter much larger than their thickness (having a ratio of almost 10), the z component of the magnetization vector is assumed to be 0. This assumption simplifies the LLG equation as follows:

$$\frac{dm_x}{dt} = \gamma\left(H_{\text{eff}_z} m_y\right) - \alpha\gamma\left(H_{\text{eff}_y} m_x m_y - H_{\text{eff}_x} m_y^2\right) \quad (11)$$

$$\frac{dm_y}{dt} = \gamma\left(-H_{\text{eff}_z} m_x\right) - \alpha\gamma\left(H_{\text{eff}_x} m_x m_y - H_{\text{eff}_y} m_x^2\right) \quad (12)$$

where $\vec{m}$ is the normalized magnetization vector and $m_x = \cos\theta$, $m_y = \sin\theta$. The effective fields are

$$H_{\text{eff}_x} = -\frac{1}{\mu_0 M_s \Omega}\frac{dE}{dm_x} + H_{\text{ext}_x} \quad (13)$$

$$H_{\text{eff}_y} = -\frac{1}{\mu_0 M_s \Omega}\frac{dE}{dm_y} + H_{\text{ext}_y} \quad (14)$$

$$H_{\text{eff}_z} = H_{\text{ext}_z}. \quad (15)$$

By plugging (3)–(8) in (14) and (15), we obtain the following:

$$\begin{aligned}
H_{\text{eff}_x} = &\left(\frac{M_s \Omega}{4\pi R^3 \sin\theta_{i,j}}\right)\Big[2\cos\theta_{i,j-1}\sin\theta_{i,j} + \sin\theta_{i,j-1}\cos\theta_{i,j} \\
&+ 2\cos\theta_{i,j+1}\sin\theta_{i,j} + \sin\theta_{i,j+1}\cos\theta_{i,j} \\
&- 2\sin\theta_{i-1,j}\cos\theta_{i,j} - \cos\theta_{i-1,j}\sin\theta_{i,j} \\
&- 2\sin\theta_{i+1,j}\cos\theta_{i,j} - \cos\theta_{i+1,j}\sin\theta_{i,j}\Big] \\
&- M_s\left(N_{d_{xx}} - N_{d_{yy}}\right)\cos\theta_{i,j} \\
&- \left(\frac{3}{\mu_0 M_s}\right)\lambda_s \sigma\cos\theta_{i,j} + H_{ext_x} \quad (16)
\end{aligned}$$

$$\begin{aligned}
H_{\text{eff}_y} = &-\left(\frac{M_s \Omega}{4\pi R^3 \cos\theta_{i,j}}\right)\Big[2\cos\theta_{i,j-1}\sin\theta_{i,j} + \sin\theta_{i,j-1}\cos\theta_{i,j} \\
&+ 2\cos\theta_{i,j+1}\sin\theta_{i,j} + \sin\theta_{i,j+1}\cos\theta_{i,j} \\
&- 2\sin\theta_{i-1,j}\cos\theta_{i,j} - \cos\theta_{i-1,j}\sin\theta_{i,j} \\
&- 2\sin\theta_{i+1,j}\cos\theta_{i,j} - \cos\theta_{i+1,j}\sin\theta_{i,j}\Big] \\
&+ M_s\left(N_{d_{xx}} - N_{d_{yy}}\right)\sin\theta_{i,j} \\
&- \left(\frac{3}{\mu_0 M_s}\right)\lambda_s \sigma\sin\theta_{i,j} + H_{\text{ext}_y} \quad (17)
\end{aligned}$$

$$H_{\text{eff}_z} = H_{\text{ext}_z}. \quad (18)$$

Now in order to obtain a mechanism to numerically evaluate the angle θ_3 we need to put $m_x = \cos\theta$ and $m_y = \sin\theta$ in (11) and (12). This yields the following expression:

$$\begin{aligned}
-\sin\theta_{i,j}\frac{d\theta_{i,j}}{d}t &= \gamma\left(H_{ef\,f_z}\sin\theta_{i,j}\right) \\
&\quad - \alpha\gamma\left(H_{ef\,f_y}\cos\theta_{i,j}\sin\theta_{i,j} - H_{ef\,f_x}\sin^2\theta_{i,j}\right). \quad (19)
\end{aligned}$$

The effective fields and the above expression derived from the LLG equation need to be numerically solved to demonstrate

the switching of the central nanomagnet, hence the evaluation of the majority gate.

E. Clocking

The proposed clocking schemes can be grouped into two categories: local clocking and global clocking. Global clocking suggests that all nanomagnets in a system are disturbed out of the equilibrium state and their magnetizations are forced along the hard axis, to the high energy state via a global agent such as global magnetic field [5]. When the clock is relaxed (i.e., the global magnetic field is removed), nanomagnets align themselves to the lowest energy states, supposedly according to the inputs, thereby enabling data propagation and evaluation. However, this method is not preferred for large-scale integration since this method does not allow pipelining of data and results in frustrations (wrong switching behavior) for large arrays of nanomagnets if the applied field changes too quickly or the switching field distribution of the nanomagnets is too wide [5], [10].

In the local clocking scheme, a local agent is used to individually change the equilibrium state of the nanomagnets. In this way, nanomagnets can be relaxed sequentially, thereby reducing the chance of frustration significantly.

In this paper, we evaluate the technology using two clocking schemes that allow very dense pipelining. The clocking schemes of interest are three- and four-phase overlapping clocks [11]. These schemes are implemented such that nanomagnets are held at ready state for computation until the computational edge of the clock wave propagates through the unit.

When the computational clock edge reaches the nanomagnet, it is relaxed from the ready state and it aligns itself with its neighbor, which was just relaxed before it due to the dipole-dipole interactions. This way the data propagates along with the computational edge of the clock. Fig. 3 shows the clocking schemes. The following section shows how data propagates in horizontal and binary wires as well as majority gates under the influence of three- and four-phase clocking schemes. Figs. 4–7 show how nanomagnets are assigned different clock phases.

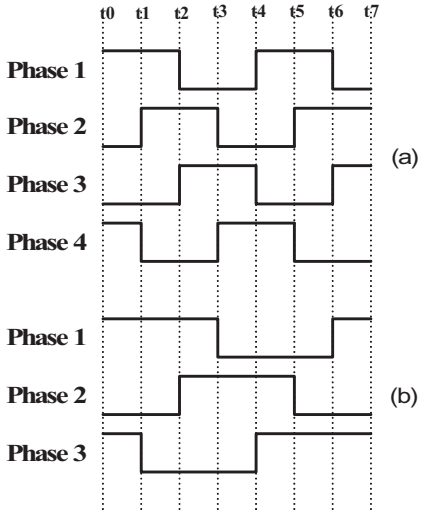

Fig. 3. Clocking schemes. (a) Four-phase clocking. (b) Three-phase clocking.

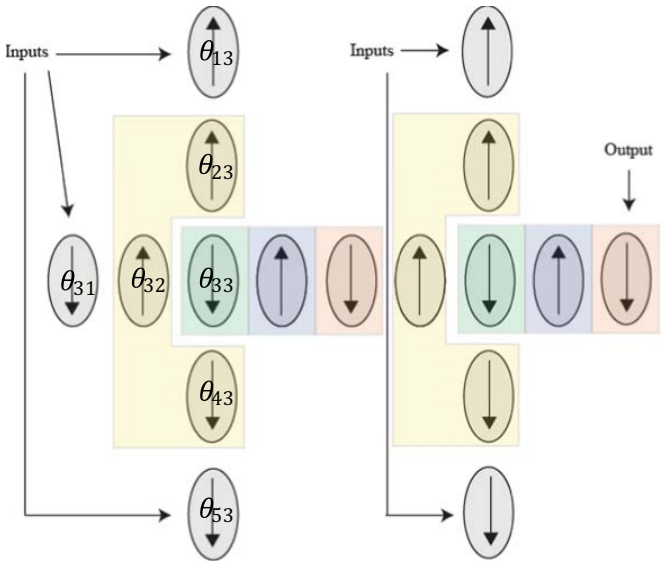

Fig. 4. Two cascaded majority gates. Four-phase clocking shown: yellow phase 1, green phase 2, blue phase 3, orange phase 4.

III. Simulation Results

A. Methodology

In our simulations, we assume the nearest neighboring couplings in both the horizontal and vertical directions. We simulate two cascaded majority gates (Fig. 4) to show the pipelining functionality since majority gates are the most complex of the three basic building blocks.

The clock-high signal represents application of compressive stress, and the clock-low signal represents application of tensile stress. The application of tensile stress is preferred, especially for high-frequency operation, because the self-relaxation of nanomagnets takes very long time and becomes the constraint on clock frequency.

B. Results

Our simulations showed that switching delays for the majority gate are not equal for all input combinations. We have considered only the input combinations that yield the worst-case switching delay in our results to obtain the required clock periods for correct operation or data propagation.

In relaxed state, when no stress is applied, nanomagnets are aligned in one of the two stable states due to their inherent shape anisotropy. We have simulated the case where the initial alignment of the nanomagnets such that all the nanomagnets need to switch in order for the data to evaluate and propagate to output. This way we could evaluate the worst-case switching scenarios and the functionality.

Another result we have obtained from our simulations is that it is not possible to obtain a working majority gate when the output is ferromagnetically coupled. The reason behind this result is that when the center and bottom nanomagnets are stressed, the effective field acting on the center nanomagnet approaches to zero magnitude as the magnetization angle of the nanomagnet approaches to 0°. At this point, dipole-dipole interactions due to neighboring nanomagnets are not enough

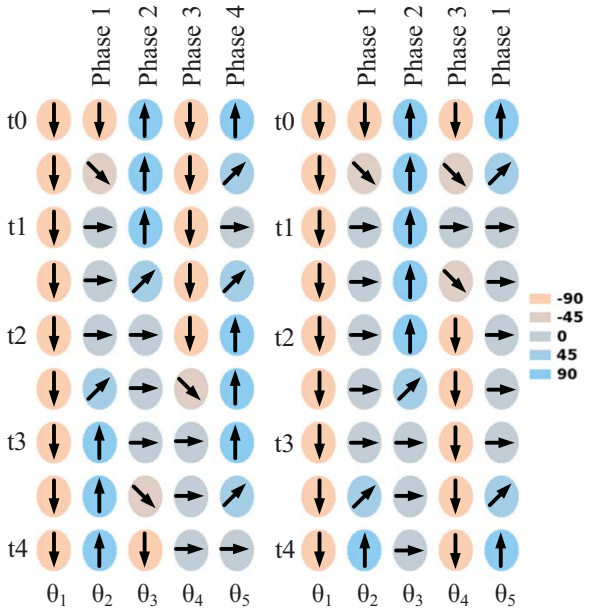

Fig. 5. Four- and three-phase clocked antiferromagnetically coupled binary wire data propagation.

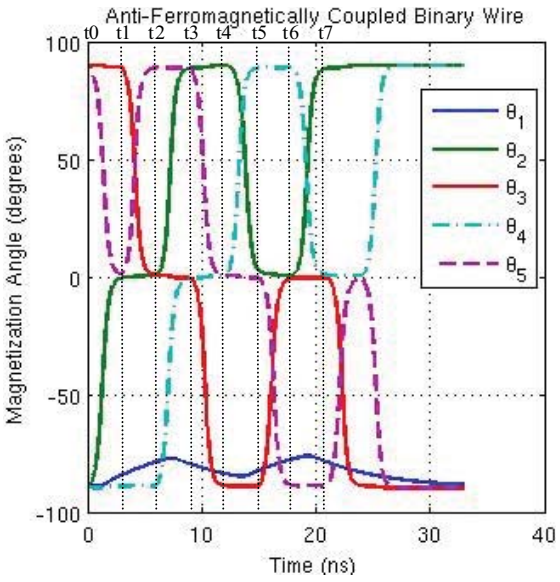

Fig. 6. Antiferromagnetically coupled binary wire data propagation.

to cross the magnetization of the nanomagnet over the hard axis barrier. This result can be analytically verified through the effective field equations.

Fig. 5 shows data propagation in antiferromagnetically coupled binary wire for the four- and three-phase clocking schemes. The figure also shows how the clock phases should be assigned to the nanomagnets to achieve the pipelined data propagation. The magnetization angles at times t_1 through t_4 are shown. The clocking schemes allow the simultaneous stressing of two neighboring nanomagnets, allowing the reduction of dipolar coupling between them. Then, the clocking allows the release of the first nanomagnet while keeping the second one stressed. This way the released nanomagnet aligns itself with its unstressed neighbor, allowing data propagation

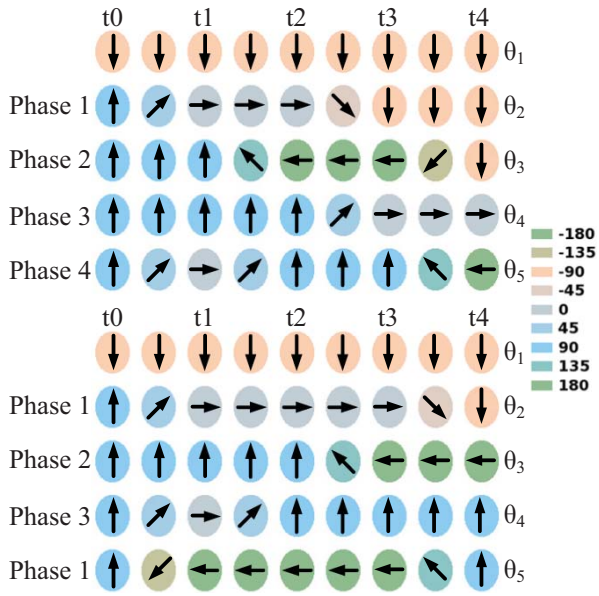

Fig. 7. Four- and three-phase clocked ferromagnetically coupled binary wire data propagation.

since the dipolar coupling between the two is now stronger than the coupling between the released nanomagnet and the stressed nanomagnet.

Fig. 6 shows the change of magnetization angles of nanomagnets over time in antiferromagnetically coupled binary wire using the four-phase clocking scheme. The clock period is chosen to be 12 ns and the applied stress is 40 MPa. The nanomagnets are annotated based on their magnetization angles in Fig. 1. θ_1 is the input nanomagnet and assumed to have switched to "0" at time t_0 and is not clocked. θ_2 is initially "0" and the remaining nanomagnets are aligned opposite to their neighbors. θ_2 is clocked with phase 1, θ_3 is clocked with phase 2, θ_4 is clocked with phase 3, and θ_5 is clocked with phase 4. θ_2 switches to "1" at time t_2, θ_3 switches to "0" at time t_3, θ_4 switches to "1" at time t_4, and θ_5 switches to "0" at time t_5.

In Fig. 7, data propagation in four- and three-phase clocked ferromagnetically coupled binary wires and how the clocks should be assigned to nanomagnets are shown. The magnetization angles at times t_1 through t_4 are shown.

Fig. 8 shows data propagation in ferromagnetically coupled binary wire with the four-phase clocking scheme. The clock period and the applied stress are the same as in the previous case. Initially, all nanomagnets are aligned in the "1" direction while the input θ_1 is aligned in the "0" direction. As the clock pulses are applied, nanomagnets start switching.

The simulation indicates that some nanomagnets switch right toward 0°, while the others switch left toward 180°. The final angle of the latter is 270°, which is the same as the desired "0" (−90°) direction. The final angles indicate if the nanomagnets switched to the left or right directions.

In Fig. 9, four-phase clocked majority gate operation is shown for continuous time. In Fig. 10, majority gate operation is shown in finite time steps for four- and three-phase clocking schemes. Clocking groups of the nanomagnets are shown in Fig. 4.

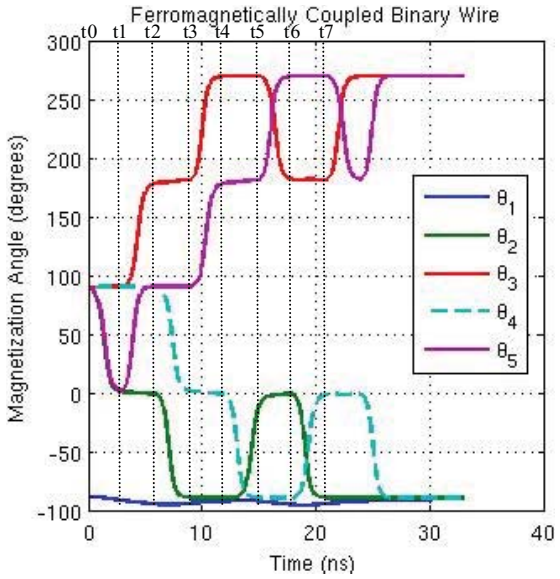

Fig. 8. Ferromagnetically coupled binary wire data propagation.

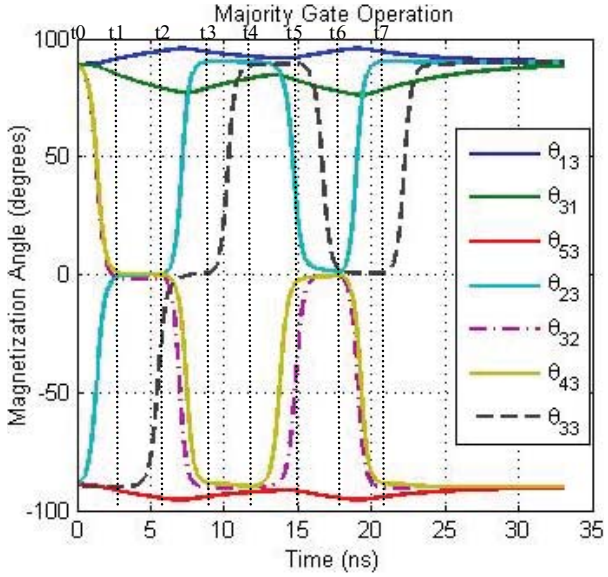

Fig. 9. Majority gate operation.

Inputs are θ_{13}, θ_{31}, and θ_{53}, are "1," "1," and "0," respectively. Input neighbors θ_{23}, θ_{32}, and θ_{43}, switch at time t_1 and the center nanomagnet θ_{33} switches at time t_2. The remaining nanomagnets are not shown since the data propagation is identical to the antiferromagnetically coupled binary wire case.

Figs. 11 and 12 show minimum clock periods required for correct operation in three components. The results indicate that the majority gate worst-case switching characteristics show about 30% degradation in comparison to the horizontal (antiferromagnetically coupled) binary wire in the three- as well as four-phase clocking schemes. Both clocking schemes result in similar clock periods. This is expected since each nanomagnet switches once every clock period in both schemes, and the clock period is limited by the switching delays of these nanomagnets. Even though the three-phase clocking scheme results in slightly worse performance, it might still be desirable since it requires one less clock phase generation.

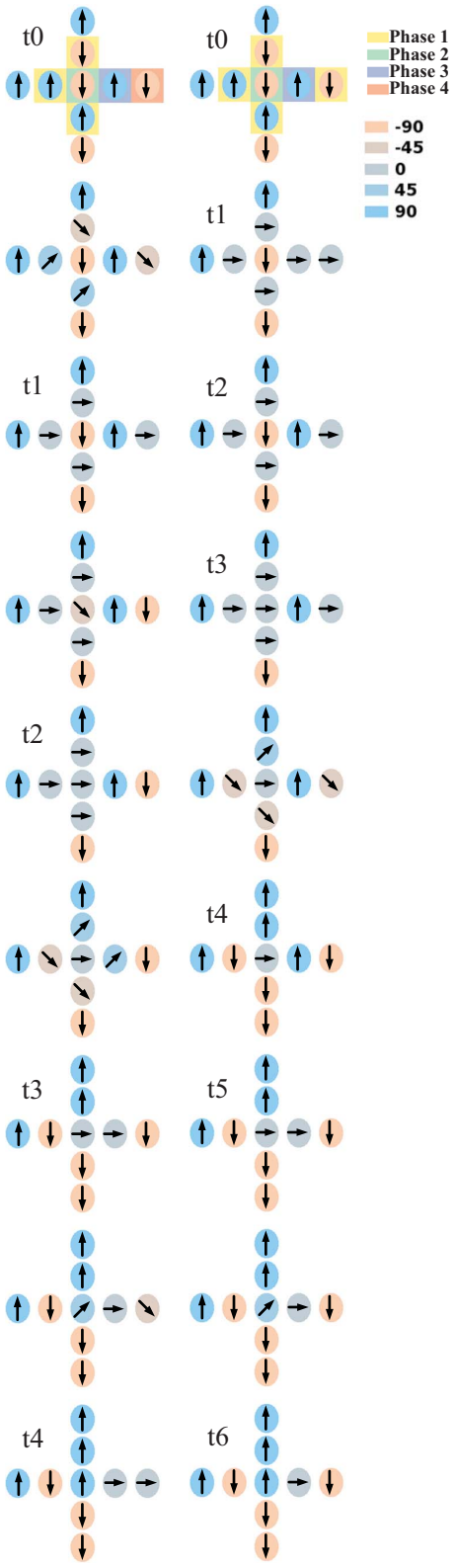

Fig. 10. Four- and three-phase clocked majority gate data propagation.

C. Energy Dissipation

Energy dissipated for switching a ferromagnetic nanomagnet is significantly less than the energy dissipated during the clock switching due to the fact that the shape anisotropy energy of the nanomagnet is less than the required energy

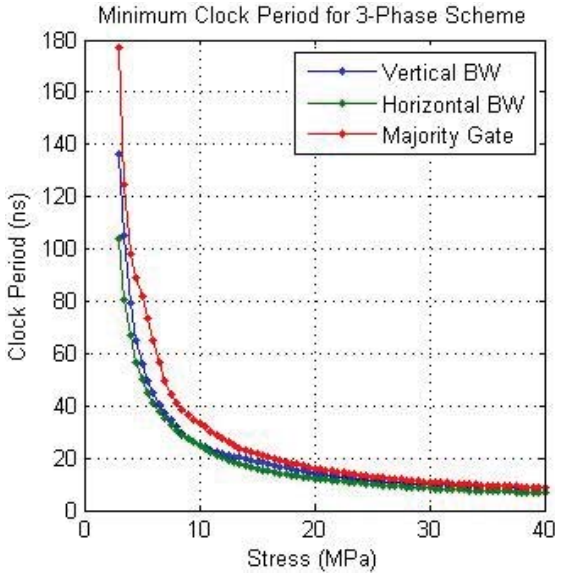

Fig. 11. Minimum clock period required for three-phase scheme to enable correct data propagation.

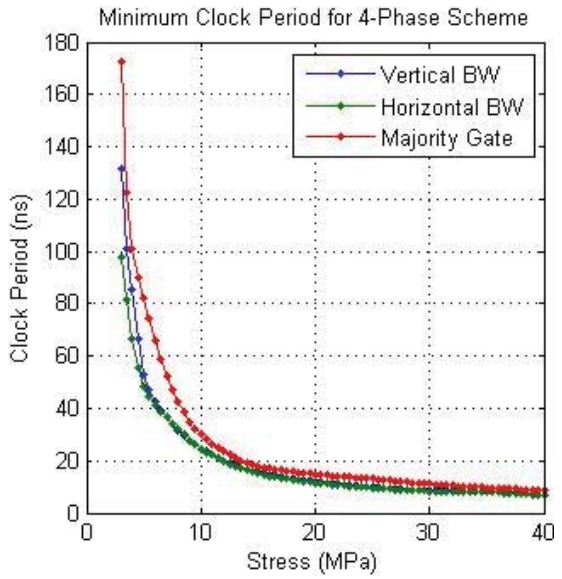

Fig. 12. Minimum clock period required for four-phase scheme to enable correct data propagation.

to generate potential difference across the PZT layer for the required stress. Therefore, power dissipated during the charging and discharging of the PZT layer needs to be considered in power estimations.

The energy dissipated during the stressing of a single nanomagnet is $E_{\text{dis}} = (1/2)CV^2$, where C is the capacitance of the PZT layer and V is the voltage required to generate desired strain by the PZT layer [3]. This value is calculated using the piezoelectric coefficient of PZT and the applied stress. V is calculated to be 111 mV to generate 40 MPa and $\sim$8.3 mV to generate 3 MPa stress. Since the nanomagnet is applied reverse stress during relaxation, the total dissipation becomes CV^2. The estimations do not include the potential consumption of driving (external) circuitry and are only based on numerical calculations.

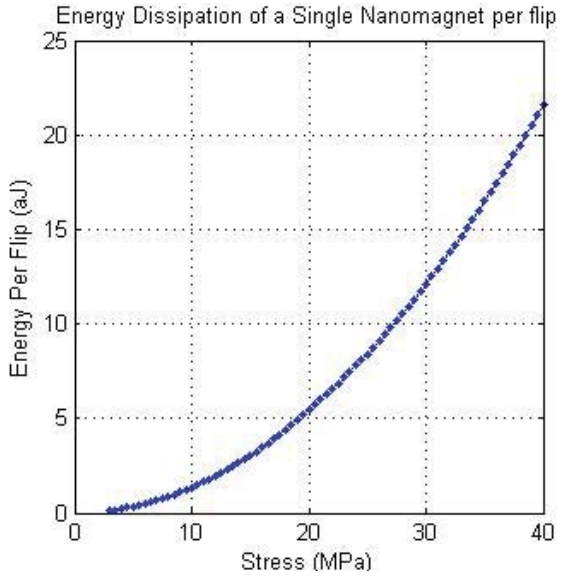

Fig. 13. Energy dissipation of single nanomagnet per flip.

Power dissipation can be estimated as the total energy times the clock frequency. Assuming all logic is clocked during the operation, even if nanomagnets do not have to switch to the opposite state, all nanomagnets are stressed. Thus, the activity factor is 1 as long as the clock signal is applied to the component.

Fig. 13 shows the energy dissipation of a single nanomagnet as a function of the applied stress. The energy dissipation does not depend on the applied clock period; it rather depends on the applied voltage across the PZT layer. Therefore, the energy dissipation depends on the applied stress on the magnetostrictive layer, by disregarding any losses during the stressing process.

IV. Discussion

The 2-D micromagnetic simulation model for the switching dynamics used in this paper does not account for the fact that the O-Φ coupled dynamics in the LLG equation causes the magnetization vector to rise above the magnetization plane. The results reported in [6] indicate that the modeling of 3-D dynamics provides faster magnetic switching and lower energy requirement for bit reversal owing to strain-assisted magnetic vector rotation by the second 90° after the external electrical pulse is removed or reversed in polarity.

However, generally, LLG-based simulation techniques for the single nanomagnet tend to underestimate the energy consumption due to their inability to model the magnetic back annotations that capture the interference effects of other nanomagnets and nonidealities in the system. Unlike in electrical design of RC-based IC circuits where parasitic extraction tools enable us to include the layout and proximity effects of other circuit elements as well as leakage effects, the energy estimation method used in this paper precludes such effects, thereby somewhat underestimating the actual energy consumed by the system. Therefore, even a micromagnetic simulator with 3-D dynamics may not be able to estimate the actual energy dissipation when magnetic back annotation tools are not available.

V. Conclusion

This paper demonstrated how nanopipelining at the nanomagnet level could be implemented using multiferroic single-domain nanomagnets. The paper also addressed the data propagation in ferromagnetically and antiferromagnetically coupled binary wires, along with a three-input majority gate operation. These devices also provided the option of trade-off between energy and performance. The energy dissipation per nanomagnet per flip was plotted as a function of the applied stress. For example, at 5-MPa stress, the energy required to flip a nanomagnet was merely 0.5 atto Joule (aJ). Preliminary studies reported in this paper boded very well for the future ultralow energy nonvolatile logic circuits, which would seek myriad applications in implants and prosthesis where the battery size and longevity were paramount.

Acknowledgment

The authors would like to thank their colleagues, especially S. Bandyopadhyay at Virginia Commonwealth University, Richmond, for encouraging them to work on this nascent straintronics-based nanomagnetic technology.

References

[1] A. Orlov, A. Imre, L. Ji, G. Csaba, W. Porod, and G. H. Bernstein, "Magnetic quantum-dot cellular automata: Recent developments and prospects," *J. Nanoelectron. Optoelectron.*, vol. 3, no. 1, pp. 55–68, 2008.

[2] S. A. Wolf, L. Jiwei, M. R. Stan, E. Chen, and D. M. Treger, "The promise of nanomagnetics and spintronics for future logic and universal memory," *Proc. IEEE*, vol. 98, no. 12, pp. 2155–2168, Dec. 2010.

[3] J. Atulasimha and S. Bandyopadhyay, "Bennett clocking of nanomagnetic logic using multiferroic single-domain nanomagnets," *Appl. Phys. Lett.*, vol. 97, no. 17, pp. 173105-1–173105-3, 2010.

[4] N. Rizos, M. Omar, P. Lugli, G. Csaba, M. Becherer, and D. Schmitt-Landsiedel, "Clocking schemes for field coupled devices from magnetic multilayers," in *Proc. 13th Int. Workshop Comput. Electron.*, May 2009, pp. 1–4.

[5] G. Csaba, A. Imre, G. H. Bernstein, W. Porod, and V. Metlushko, "Nanocomputing by field-coupled nanomagnets," *IEEE Trans. Nanotechnol.*, vol. 1, no. 4, pp. 209–213, Dec. 2002.

[6] M. S. Fashami, K. Roy, J. Atulasimha, and S. Bandyopadhyay, "Magnetization dynamics, Bennett clocking and associated energy dissipation in multiferroic logic," *Nanotechnology*, vol. 22, no. 15, p. 155201, Apr. 2011.

[7] T. Brintlinger, S.-H. Lim, K. H. Baloch, P. Alexander, Y. Qi, J. Barry, J. Melngailis, L. Salamanca-Riba, I. Takeuchi, and J. Cumings, "In situ observation of reversible nanomagnetic switching induced by electric fields," *Nano Lett.*, vol. 10, no. 4, pp. 1219–1223, Mar. 2010.

[8] T. K. Chung, S. Keller, and G. P. Carman, "Electric-field-induced reversible magnetic single-domain evolution in a magnetoelectric thin film," *Appl. Phys. Lett.*, vol. 94, no. 13, pp. 132501-1–132501-3, Mar. 2009.

[9] J. F. Pulecio and S. Bhanja, "Magnetic cellular automata wires," in *Proc. IEEE Nanotechnol. Mater. Devices Conf.*, Jun. 2009, pp. 73–75.

[10] A. Kumari and S. Bhanja, "Magnetic cellular automata (MCA) arrays under spatially varying field," in *Proc. IEEE Nanotechnol. Mater. Devices Conf.*, Jun. 2009, pp. 50–53.

[11] C. Augustine, B. Behin-Aein, X. Fong, and K. Roy, "A design methodology and device/circuit/architecture compatible simulation framework for low-power magnetic quantum cellular automata systems," in *Proc. Asia South Pacific Design Autom. Conf.*, Jan. 2009, pp. 847–852.

Yalcin Yilmaz received the B.S. and M.S. degrees in electrical engineering from the University of Michigan, Ann Arbor, in 2009 and 2011, respectively, where he is currently pursuing the Ph.D. degree in electrical engineering.

He is a graduate student Research Assistant with the Department of Electrical Engineering and Computer Science, University of Michigan. His current research interests include modeling, simulation, and low-power circuit designs for emerging technologies, including spin-based devices.

Pinaki Mazumder (S'84–M'88–SM'94–F'99) is currently with the Department of Electrical Engineering and Computer Science, University of Michigan, Ann Arbor. He was a Research Assistant with the Coordinated Science Laboratory, University of Illinois at Urbana-Champaign, Urbana, for two years, and was with Bharat Electronics Ltd. (a collaborator of RCA), Bangalore, India, for over six years, where he developed several types of analog and digital integrated circuits for consumer electronics products. In 1985 and 1986, he was a Technical Staff member with Indian Hill Branch, AT&T Bell Laboratories, Murray Hill, NJ. From 1996 to 1997, he was a Visiting Faculty member with Stanford University, Stanford, CA, the University of California, Berkeley, and Nippon Telephone and Telegraph, Tokyo, Japan. From 2007 to 2009, he served as the Lead Program Director with the CISE and ENG Directorates, U.S. National Science Foundation. He has authored or co-authored over 250 papers on these topics in archival journals and proceedings of the international conferences. He has led his research group's efforts in VLSI testing and built-in self-repair techniques and has developed silicon compilers for RAM, ROM, and programmable logic array with built-in self-repairable capabilities. He has done extensive work in the area of VLSI physical design. He has developed a suite of distributed place-and-route tools for VLSI and field-programmable gate array chips. He has developed CAD tools for high-performance VLSI circuit simulation (NDR-SPICE) and numerous circuit topologies for quantum mortgage operating system and other quantum-well devices. He is the co-author of *Testing and Testable Design of High-Density Random-Access Memories* (Kluwer, 1996), *Semiconductor Random-Access Memories: Testing and Reliability* (Computer Science, 1998), *Genetic Algorithms for VLSI Design, Layout, and Test Automation* (Prentice-Hall, 1998).

He was a recipient of the Digital's Incentives for Excellence Award, the BF Goodrich National Collegiate Invention Award, the National Science Foundation Research Initiation Award, and the Bell Northern Research Laboratory Faculty Award. He was a Guest Editor for the IEEE Design and Test Magazine's Special Issue on Multi Megabit Memory Testing in 1993, and the Journal of Electronic Testing: Theory and Applications Special Issue on Memory Testing and Reliability in 1994. He was the Guest Editor of two special issues on Emerging Nanoelectronic Technologies and their applications in the IEEE Transactions on Very Large Scale Integration (VLSI) Systems in 1997, the IEEE Transactions on Computers in 2010, and the Proceedings of the IEEE in 1998 and 2012. He is on the Editorial Board of Proceedings of the IEEE and is an Associate Editor of the IEEE Transactions on Very Large Scale Integration (VLSI) Systems. In 2007, he was elected a fellow of the American Association of Advancements in Science.